IEEE Access
Multidisciplinary | Rapid Review | Open Access Journal

Received July 15, 2019, accepted August 2, 2019, date of publication August 12, 2019, date of current version September 23, 2019.

*Digital Object Identifier 10.1109/ACCESS.2019.2934744*

# Design of a New N-Shape Composite Ultra-Thin Deployable Boom in the Post-Buckling Range Using Response Surface Method and Optimization

**HUI YANG[1], FENGSHUAI LU[1], HONGWEI GUO[2], AND RONGQIANG LIU[2]**

[1]College of Electrical Engineering and Automation, Anhui University, Hefei 230601, China
[2]China State Key Laboratory of Robotics and System, Harbin Institute of Technology, Harbin 150001, China

Corresponding author: Hongwei Guo (guohw@hit.edu.cn)

This work was supported in part by the key Funds of the National Natural Science Foundation of China under Grant 51835002, in part by the National Natural Science Foundation of China under Grant 51605001, in part by the Joint Funds of the National Natural Science Foundation of China under Grant U1637207, and in part by the Key Research and Development Plan of Anhui Province, China, under Grant 201904A05020034.

**ABSTRACT** Composite ultra-thin boom can be folded elastically. Moreover, such booms are able to self-deploy by releasing stored strain energy, which can be applied in deployable antenna, solar sail, and optical telescopes. Surrogate models for imperfection-sensitive quantities of interest and multi-objective optimization are developed for the design of a new N-shape cross-section composite ultra-thin deployable boom. The proposed optimal design method integrates four general steps: (1) design of experiments, wherein the sampling designs of the N boom are created on the basis of the two-factor five-level full factorial design of experiments method; (2) efficient computational analyses of each design sample, wherein the post-buckling behavior of the N boom are analyzed under three different axial directions using nonlinear finite element ABAQUS/Explicit solver; (3) establishing the surrogate models of bending stiffness around the $x$-and $y$- axes and torsional stiffness around the $z$-axis by response surface method (RSM); (4) performing the multi-objective optimization design using modified non-dominated sorting genetic algorithm to realize the optimal design. The bending stiffness around the $x$-and $y$- axes and the torsional stiffness around the $z$-axis are set as the objectives, mass is set as the constraint, and the bonded web height and the central angle of the middle tape spring of the N boom are set as the variables. The typical surrogate modeling method can be applied to different problems in structural and material design.

**INDEX TERMS** Deployable structures, N boom, buckling, response surface method, optimization.

## I. INTRODUCTION

Deployable structures, such as solar sails, antennae and optical telescopes, have been essential for space applications because of the limited volume of launching vehicles and the large-scale operating requirements in space. Different cross section wrapping deployable booms, such as the lenticular boom [1]–[3], triangular rollable and collapsible (TRAC) boom [4], [5], and storable tubular extendable member (STEM) [6], [7], have also been developed for spatial applications. All three booms can be wrapped around a hub, whereby the booms transitions from a flattened configuration to a structurally deployed shape.

Theoretical and experimental study on deployable truss structures were conducted [8]. An active-passive composite for driving a deployable lenticular boom for space probes was proposed and tested [9], and a geometrical optimal design of the lenticular boom was developed though modal and coiling analysis [10], [11]. A double-layer tape spring and integral tube hinge with double slots were investigated on basis of the response surface (RS) method [12]–[14]. A hinge that consists of three single tape springs was tested, and the finite element (FE) model was validated by the physics-based simulation results [15], [16]. The micro-mechanical behavior of two-ply plain weave laminates under small strains

The associate editor coordinating the review of this article and approving it for publication was Hao Luo.

for deployable booms was predicted [17]. The post-buckling characteristics of slender structures demonstrated an important relationship with loading capacity [18]. Stress concentration and material failure during the coiling of the TRAC boom were tested [19]. The bending and torsional behaviors of the TRAC booms were studied using numerical analysis and experimental testing [20]. The TRAC boom could carry significantly increased loads well into the post-buckling regime, and a data-driven computational framework improved their buckling and post-buckling behavior through [21], [22]. The STEM and lenticular booms were effectively derived, and their thickness was calculated under the assumption of a strain of 1.5%. The TRAC boom obtained 10 times more cross-section inertia than the lenticular boom and 34 times more than the STEM boom at the same packaged height [23]. However, the TRAC boom with open section demonstrated remarkably lower torsional stiffness than the closed section thin-walled boom.

This work aims to propose a new N-shape cross section (N) boom and to assess structural bending and torsional stiffness throughout the entire post-buckling process around the three axes. The N composite ultra-thin deployable boom, which has a configuration similar to that of the TRAC boom, consists of three tape springs. The middle tape spring has two circumscribed circles and two adjacent tape springs that bond along one longitudinal edge of the C shapes. Moreover, the torsional stiffness of the N boom is greater than that of the TRAC boom. The structural bending and torsional stiffness throughout the entire post-buckling process around the three axes should be analyzed to increase the capacity of the N boom in deploying state. Section 2 describes the behaviors of the N booms in detail. Section 3 presents a method using the RS theory to establish the surrogate model of the bending stiffness around the $x$- and $y$- axes and the torsional stiffness around the $z$-axis. The two-factor five-level full factorial design of experiment (DoE) is applied to obtain the sample points. Accuracy analysis validated the surrogate models. Section 4 presents the multi-objective optimization. Section 5 discusses the results and concludes the study.

## II. BEHAVIOR OF THE N DEPLOYABLE BOOMS

The N boom is similar to the TRAC boom, which also consists of two tape springs that bond along one longitudinal edge of the C shapes. The difference between these two types of booms is that the N boom consists of three tape springs, in which the middle tape spring has two circumscribed circles. Coordinate system of the N boom cross-section is shown in Figure.1. The N boom is centrosymmetric with respect to the $y$-axis. The bonded web height is $h$, and the thickness of each tape spring is $t_n$. The radius and central angle of the outer side tape spring are $R_1$ and $\theta_1$, respectively; and those of the internal side tape spring are $R_2$ and $\theta_2$, respectively. The N boom is made by laying four plies [45°/−45°/45°/−45°] of T800 carbon fiber reinforced polymer as shown in Figure.2. Each ply thickness is $t_0 = 0.125$ mm, each tape spring thickness is 0.5-mm, and the longitudinal length is $L_n = 1$ m.

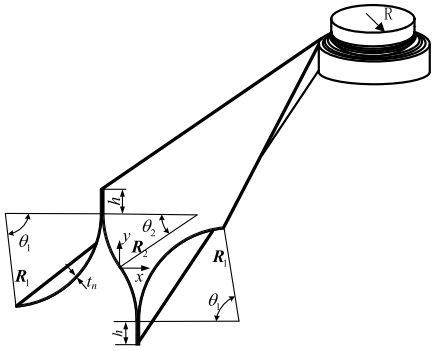


**FIGURE 1.** Cross section geometrical dimension of the N boom.

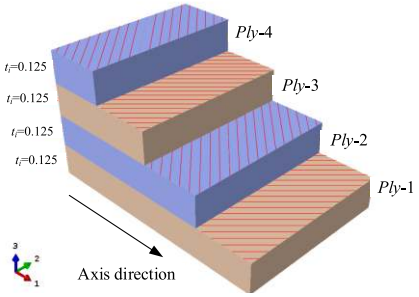


**FIGURE 2.** Material layout of the four plies [45°/ − 45°/45°/ − 45°].

**TABLE 1.** Material properties of T800 and cohesive glue.

| Material Properties | T800 | Glue |
|---|---|---|
| Longitudinal stiffness $E_1$ /MPa | 150 000 | - |
| Transverse stiffness $E_2$=$E_3$ /MPa | 7 000 | 60000 |
| Shear stiffness $G_{12}$=$G_{13}$ /MPa | 7 000 | - |
| In-plane shear stiffness $G_{23}$ /MPa | 4 500 | - |
| Poisson's ratio $\upsilon$ | 0.3 | 0.3 |
| Density $\rho$ kg/m$^3$ | 2 500 | 1600 |

Two webs are bonded by cohesive glue. Material properties of T800 and glue are listed in Table 1.

The longitudinal length ($L_n = 1$ m) and thickness ($t_n = 0.5$ mm) are kept constant, and the same composite material described previously with the stacking sequence of [45°/ − 45°/45°/ − 45°] is considered. The cross section width of the flattening tape springs is kept constant for all the three tape springs in each N boom to establish a fair comparison between different geometries. Figure.1 shows that the flattening width constant introduces a relationship among the one internal and two external tape springs and two independent parameters (e.g., $h$ and $\theta_2$) considered in this study:

$$\theta_1 = \frac{2R_2\theta_2 + h}{R_1} \tag{1}$$

N boom mass is presented as follows:

$$Mass\,(h, \theta_2) = 6\rho \cdot L_n \cdot t_n\,(R_2\theta_2 + h) \tag{2}$$

**TABLE 2. Boundary conditions of RP2 under different circumstances.**

| | Bend around $x$-axis | Bend around $y$-axis | Torsion around $z$-axis |
|---|---|---|---|
| UX | 0 | Free | Free |
| UY | Free | 0 | Free |
| UZ | Free | Free | 0 |
| RX | Loading | 0 | 0 |
| RY | 0 | Loading | 0 |
| RZ | 0 | 0 | Loading |

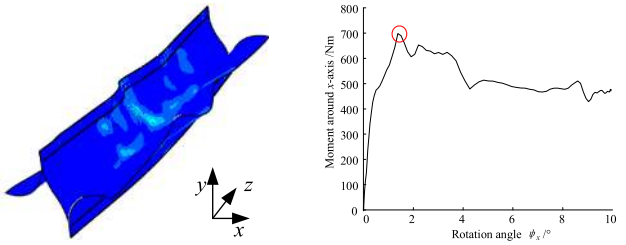


**FIGURE 3. Predicted responses for the N boom: (a) bending moment around X; (d) $M_x - \psi_x$.**

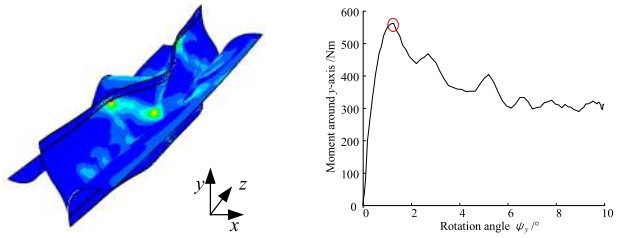


**FIGURE 4. Predicted responses for the N boom: (a) bending moment around Y; (d) $M_x$-$\psi_y$.**

FE models are set up in the ABAQUS/Explicit software. Four nodes fully reduced integrated shell elements (S4R) and eight nodes three-dimensional cohesive elements (COH3D8) are applied. Two reference points (e.g., RP1 and RP2) are located on either end and set as the kinematic coupling constraints to either end surface. The degrees of freedom on RP1 are all restrained. The boundary conditions of RP2 under different circumstances are listed in Table 2. When buckling occurs in the N boom, the maximum moment around the three axes and the corresponding angle of rotation can be extracted. Figures 3-5 shows the predicted responses for the idealized N boom with $h = 35$ mm and $\theta_2 = 40°$.

The ultimate buckling limit of the N boom is reached at the first bifurcation point, and the ultimate buckling limit is selected as the analytical maximum moment in the moment-angle response of the N boom. Thus, bending stiffness $EI_x\,(h, \theta_2)$, $EI_y\,(h, \theta_2)$ around the $x$-axis and $y$-axis, and torsional stiffness around the $z$-axis can be derived:

$$EI_x\,(h, \theta_2) = \left(\frac{dM_x}{d\theta_x}\right) \cdot L_n \tag{3}$$

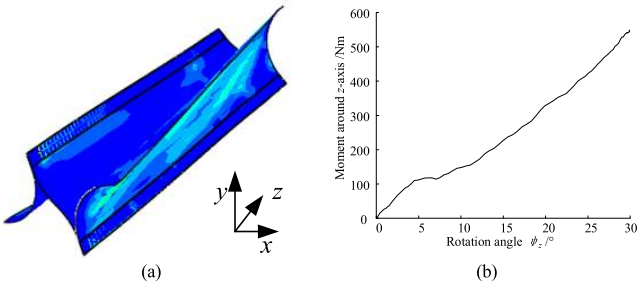


**FIGURE 5. Predicted responses for the N boom: (a) bending moment around Z; (d) $M_x - \psi_z$.**

$$EI_y\,(h, \theta_2) = \left(\frac{dM_y}{d\theta_y}\right) \cdot L_n \tag{4}$$

$$GJ_z\,(h, \theta_2) = \left(\frac{dM_z}{d\theta}\right) \cdot L_n \tag{5}$$

where $M_x$ is the moment around the $x$-axis, $M_y$ is the moment around the $y$-axis; $M_z$ is the moment around the $z$-axis; $\theta_x$ is the rotation angle around the $x$-axis; $\theta_y$ is the rotation angle around the $y$-axis; $\theta_z$ is the rotation angle around the $z$- axis.

## III. RESPONSE SURFACE METHOD OF THE N BOOM

### A. SAMPLE POINTS

To save computational time and cost in the buckling analysis, the RS method [24], [25] is used in the optimization study of the N boom. The RS method refers to a collection of mathematical and statistical procedures. The responses of the N booms includes the bending stiffness around the $x$-axis $EI_x(h, \theta_2)$, the bending stiffness around the $y$-axis $EI_y(h, \theta_2)$, and the torsional stiffness around the $z$-axis $GJ_z(h, \theta_2)$, which can be written in terms of a series of basic functions as follows:

$$\tilde{y}\,(h, \theta_2) = \sum_{i=1}^{n} \beta_i \varphi_i\,(h, \theta_2) \tag{6}$$

where $\tilde{y}\,(h, \theta_2)$ represents the responses of $EI_x(h,\ \theta_2)$, $EI_y(h, \theta_2)$ and $GJ_z(h, \theta_2)$; $n$ is the number of basic functions $\phi_i(h, \theta_2)$, $i$ is the number of the design variables, and $\beta_i$ is the coefficients of the basic functions. Polynomials are typical classes of basic functions, and a full $n$-order polynomial is given as

$$\begin{aligned}
&1, x_1, x_{2,\ldots} x_n,\\
&x_1^2, x_1 x_{2,} \ldots x_1 x_{n,} \ldots, x_n^2,\\
&x_1^3, x_1^2 x_2, \ldots, x_1^2 x_n, x_1 x_2^2, \ldots, x_1 x_n^2, \ldots, x_n^3\\
&x_1^4, x_1^3 x_2, \ldots, x_1^3 x_n, x_1^2 x_2^2, \ldots, x_1^2 x_n^2, \ldots, x_1 x_2^3,\\
&\quad \ldots, x_1 x_n^3, \ldots, x_n^4\\
&\vdots\\
&x_1^n, x_1^{n-1} x_2, \ldots, x_1 x_n^{n-1}, x_1^2 x_2^2, \ldots, x_1^2 x_n^{n-2},\\
&\quad \ldots, x_1 x_2^{n-1}, \ldots, x_n x_2^{n-1}, \ldots, x_n^n
\end{aligned} \tag{7}$$

**TABLE 3.** Sample points and FE results of the bending stiffness around the x-axis.

| No | $h$ /mm | $\theta_2$/° | $EI_x(h,\theta_2)$ (N·m²/rad) | $EI_y(h,\theta_2)$ (N·m²/rad) | $GJ_z(h,\theta_2)$ (N·m²/rad) |
|---|---|---|---|---|---|
| 1 | 30 | 30 | 22902.76 | 13283.30 | 309.59 |
| 2 | 30 | 32.5 | 17009.73 | 14528.21 | 454.28 |
| 3 | 30 | 35 | 20018.65 | 18717.93 | 681.46 |
| 4 | 30 | 40 | 26844.00 | 25238.69 | 1284.93 |
| 5 | 30 | 45 | 27512.57 | 35923.76 | 1392.44 |
| 6 | 35 | 30 | 25031.26 | 14799.08 | 352.65 |
| 7 | 35 | 32.5 | 18859.77 | 15173.81 | 525.32 |
| 8 | 35 | 35 | 27639.15 | 17865.24 | 714.09 |
| 9 | 35 | 40 | 32029.18 | 24863.49 | 1266.72 |
| 10 | 35 | 45 | 32672.37 | 42408.89 | 1389.49 |
| 11 | 40 | 30 | 31419.65 | 14032.93 | 335.36 |
| 12 | 40 | 32.5 | 27368.94 | 14720.85 | 533.58 |
| 13 | 40 | 35 | 29041.04 | 18292.35 | 737.51 |
| 14 | 40 | 40 | 35532.41 | 28335.39 | 1198.68 |
| 15 | 40 | 45 | 28994.20 | 45166.06 | 1374.07 |
| 16 | 45 | 30 | 25720.40 | 14930.85 | 380.68 |
| 17 | 45 | 32.5 | 27704.56 | 16681.14 | 592.02 |
| 18 | 45 | 35 | 33645.25 | 19817.28 | 688.42 |
| 19 | 45 | 40 | 31339.98 | 33052.28 | 1323.39 |
| 20 | 45 | 45 | 29900.12 | 49859.45 | 1456.44 |
| 21 | 50 | 30 | 23809.02 | 16528.52 | 433.14 |
| 22 | 50 | 32.5 | 33120.92 | 15455.37 | 594.67 |
| 23 | 50 | 35 | 37684.79 | 21045.53 | 760.79 |
| 24 | 50 | 40 | 33419.45 | 30884.09 | 1255.94 |
| 25 | 50 | 45 | 38209.31 | 43478.15 | 1441.23 |

The quartic polynomials ($n = 15$) are selected to derive the basic functions in this study to ensure the accuracy and save computational time. Several design sample points $(h, \theta_2)^{(j)}$ $(j = 1, 2, \ldots, \mathrm{m})$ are needed $(m > n)$ to determinate unknown parameters $\mathbf{b} = (\beta_1, \beta_2, \ldots, \beta_n)$ in Eq.(6). The two-factor five level full-factorial DoE point is selected, and 25 sample points are obtained. The longitudinal length $L_n = 1$ m, thickness $t_n = 0.5$ mm, and radius of the external tape springs $R_1 = 153$ mm are kept constant. The bonded web height $h$ changes from 30 mm to 50 mm, and the central angle $\theta_2$ of the middle shell changes from 30° to 45°. Sample points and FE results of the N boom are listed in Table 3.

### B. SURROGATE MODEL

From the simulation results (Table 3) and by combining Eqs. (6), (7), (8), and (9), the surrogate models of $EI_x(h, \theta_2)$, $EI_y(h, \theta_2)$, and $GJ_z(h, \theta_2)$ are derived from the DoE results,

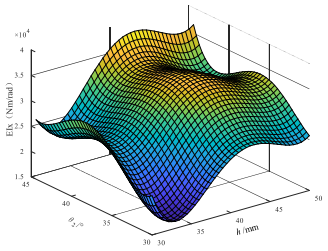

**FIGURE 6.** RS of $EI_x(h, \theta_2)$.

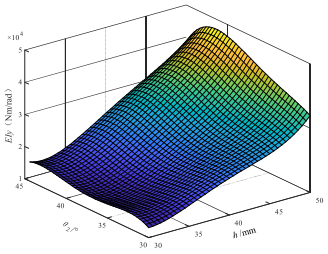

**FIGURE 7.** RS of $EI_y(h, \theta_2)$.

which are written as follows:

$$\begin{aligned} &EI_x(h, \theta_2) \\ &= 1.6955 \times 10^7 - 3.8366 \times 10^5 h - 1.4325 \times 10^6 \theta_2 \\ &\quad + 12494h^2 + 5355.6h\theta - 186.3018h^3 \\ &\quad + 54490\theta_2^2 - 92.1914h^2\theta_2 - 45.9468h\theta_2^2 \\ &\quad - 944.2703\theta_2^3 + 0.9891h^4 + 0.8501h^3\theta_2 \\ &\quad - 0.0939h^2\theta_2^2 + 0.4415h\theta_2^3 + 6.0864\theta_2^4 \end{aligned} \tag{8}$$

$$\begin{aligned} &EI_y(h, \theta_2) \\ &= -1.2496 \times 10^6 + 2.987 \times 10^5 h \\ &\quad - 1.6571 \times 10^5 \theta_2 - 7.6665 \times 10^3 h^2 \\ &\quad - 8.67 \times 103h\theta + 1.1161 \times 10^4 \theta_2^2 \\ &\quad + 99.8632h^3 + 106.5774h^2\theta_2 + 124.1173h\theta_2^2 \\ &\quad - 243.185\theta_2^3 - 0.5258h^4 - 0.4997h^3\theta_2 \\ &\quad - 0.679h^2\theta_2^2 - 0.6149h\theta_2^3 + 1.7912\theta_2^4 \end{aligned} \tag{9}$$

$$\begin{aligned} &GJ_z(h, \theta_2) \\ &= -1.9112 \times 10^5 + 4213.3h + 17135\theta_2 \\ &\quad - 170.7715h^2 + 22.7335h\theta - 744.0332\theta_2^2 \\ &\quad + 2.6029h^3 + 0.8881h^2\theta_2 - 1.6326h\theta_2^2 \\ &\quad + 14.6663\theta_2^3 - 0.0143h^4 - 0.0087h^3\theta_2 \\ &\quad + 0.0022h^2\theta_2^2 + 0.0135h\theta_2^3 - 0.1067\theta_2^4 \end{aligned} \tag{10}$$

The derived RSs for $EI_x(h, \theta_2)$, $EI_y(h, \theta_2)$ and $GJ_z(h, \theta_2)$ of the N boom are plotted in Figures 6, 7 and 8, respectively. It can be seen that $EI_x(h, \theta_2)$ is sensitive to the central angle $\theta_2$ and the bonded web height $h$, but $EI_y(h, \theta_2)$ and $GJ_z(h, \theta_2)$ are more sensitive to the bonded web height $h$ than the central angle $\theta_2$ of the middle tape spring.

### C. ACCURACY ANALYSIS

The accuracy of the surrogate models must be evaluated using several criteria, i.e., coefficient of multiple

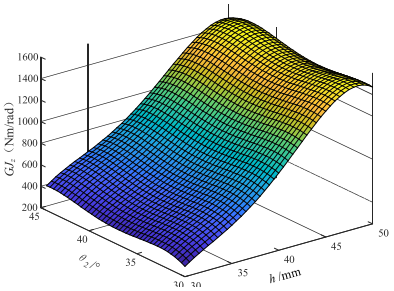


**FIGURE 8.** RS of $GJ_z\ (h, \theta_2)$.

determination ($R^2$), relative error ($RE$), root mean square error ($RMSE$), and adjusted coefficient of the multiple determination ($R^2_{adj}$). The criteria are written as follows:

$$RE = \frac{\tilde{y}_i\,(h, \theta_2) - y_i\,(h, \theta_2)}{y_i\,(h, \theta_2)} \tag{11}$$

$$R^2 = 1 - \frac{SSE}{SST} \tag{12}$$

$$R^2_{\text{adj}} = 1 - \frac{M-1}{M-N}\left(1 - R^2\right) \tag{13}$$

$$RMSE = \left(\frac{SSE}{M-N-1}\right)^{0.5} \tag{14}$$

where $y_i\,(h, \theta_2)$ is the simulation result, $SSE$ is the total sum of the squares, and $SST$ is the sum of squares of the following residuals:

$$SST = \sum_{i=1}^{M} \left[y_i\,(h, \theta_2) - \bar{y}\,(h, \theta_2)\right]^2 \tag{15}$$

$$SSE = \sum_{i=1}^{M} \left[y_i\,(h, \theta_2) - \tilde{y}\,(h, \theta_2)\right]^2 \tag{16}$$

For the surrogate models, the values of bending stiffness around the $x$-axis $EI_x\,(h, \theta_2)$, bending stiffness around the $y$-axis $EI_y\,(h, \theta_2)$, and torsional stiffness around the $z$-axis $GJ_z\,(h, \theta_2)$ vary from 0 to 1, which expresses the correlation level between the simulation results and responses. The enlarged $R^2$ and $R^2_{adj}$ and small $RE$ and $RMSE$ improve the RS fitting.

The buckling process simulation is highly nonlinear and needs high computation cost. The N boom longitudinal length is set to $L_n = 1$ m. The single flange thickness ($t_n = 0.5$ mm) and the flattening width of the three shells in each N boom are kept constant in the buckling process analysis. The $RE$ errors between the FE and RS results of the 25 selected sample points are listed in Table 4.

The accuracies of the quartic polynomial functions are calculated by substituting the approximation of the responses derived from Eqs. (8) - (10) and the simulation results into Eqs. (11) - (14) with $m = 25$ and $n = 15$. The accuracies of the different RS models for the N booms are presented in Table 5. The values of $RE$s are no more than 8.81 %, meanwhile $R^2$ and $R^2_{adj}$ are close to 1. These findings indicate that the accuracies of the surrogate models are sufficient for the selected sample points.

**TABLE 4.** RE errors between the FE models and RS results for the 25 sample points.

| No | RS results | | | RE /% | | |
|---|---|---|---|---|---|---|
| | $EI_x$ $(h,\theta_2)$ | $EI_y$ $(h,\theta_2)$ | $GJ_z$ $(h,\theta_2)$ | $EI_x$ $(h,\theta_2)$ | $EI_y$ $(h,\theta_2)$ | $GJ_z$ $(h,\theta_2)$ |
| 1 | 22751.55 | 13101.43 | 295.40 | -0.66 | -1.37 | -4.58 |
| 2 | 16443.57 | 15031.14 | 476.17 | -3.33 | 3.46 | 4.82 |
| 3 | 20922.18 | 18544.28 | 675.02 | 4.51 | -0.93 | -0.94 |
| 4 | 26933.96 | 24565.99 | 1276.68 | 0.34 | -2.67 | -0.64 |
| 5 | 27236.22 | 36449.11 | 1399.44 | -1.01 | 1.46 | 0.50 |
| 6 | 25274.60 | 14766.30 | 359.64 | 0.97 | -0.22 | 1.98 |
| 7 | 20254.64 | 15039.62 | 532.38 | 7.34 | -0.88 | 1.34 |
| 8 | 25458.43 | 18148.38 | 712.18 | -7.89 | 1.58 | -0.27 |
| 9 | 32059.88 | 25964.57 | 1267.86 | 0.096 | 4.43 | 0.089 |
| 10 | 33183.94 | 41191.70 | 1376.22 | 1.57 | -2.87 | -0.96 |
| 11 | 30523.61 | 14109.89 | 340.88 | -2.85 | 0.555 | 1.65 |
| 12 | 25691.06 | 14185.39 | 520.21 | -6.13 | -3.64 | -2.51 |
| 13 | 30460.72 | 17923.96 | 696.94 | 4.89 | -2.01 | -5.50 |
| 14 | 35157.04 | 28329.81 | 1242.78 | -1.06 | -0.019 | 3.68 |
| 15 | 30523.61 | 45998.58 | 1378.40 | 5.27 | 1.84 | 0.31 |
| 16 | 25022.61 | 15635.71 | 386.46 | -2.71 | 4.73 | 1.52 |
| 17 | 29792.69 | 16035.00 | 570.73 | 7.54 | -3.87 | -3.59 |
| 18 | 33276.88 | 20500.60 | 744.15 | -1.09 | 3.45 | 8.09 |
| 19 | 31043.42 | 32417.39 | 1283.78 | -0.95 | -1.92 | -2.99 |
| 20 | 29174.47 | 49751.51 | 1455.85 | -2.43 | -0.22 | -0.041 |
| 21 | 25355.79 | 15960.53 | 429.04 | 6.49 | -3.44 | -0.95 |
| 22 | 32154.75 | 16268.27 | 600.38 | -2.92 | 5.26 | 0.96 |
| 23 | 38307.59 | 20621.17 | 753.98 | 1.65 | -2.02 | -0.89 |
| 24 | 32154.75 | 31096.25 | 1258.58 | -3.78 | 0.67 | 0.21 |
| 25 | 38270.36 | 43445.50 | 1443.78 | 0.16 | -0.08 | 0.18 |

**TABLE 5.** Accuracy of the different RS models for the N booms.

| | $R^2$ | $R^2_{adj}$ | $RE$ /% |
|---|---|---|---|
| $EI_x$ (N·m$^2$/rad) | 0.9623 | 0.9096 | -6.13 ~ 7.54 |
| $EI_y$ (N·m$^2$/rad) | 0.9974 | 0.9938 | -3.87 ~ 5.26 |
| $GJ_z$ (N·m$^2$/rad) | 0.9976 | 0.9942 | -8.81 ~ 7.82 |

**TABLE 6.** Scale and weight factors of the objectives and constraint.

| | $S_j$ | $W_j$ |
|---|---|---|
| $EI_x$ | 1 | 0.5 |
| $EI_y$ | 1 | 0.8 |
| $GJ_z$ | 1 | 100 |
| $Mass$ | 1 | 20 |

**TABLE 7.** Feasible designs of the N boom.

| No. | $h$ /mm | $\theta_2$ /° | $EI_x$ /(Nm$^2$/rad) | $EI_y$ /(Nm$^2$/rad) | $GJ_z$ /(Nm$^2$/rad) | *Mass* /g |
|---|---|---|---|---|---|---|
| 1 | 37.153348 | 33.487733 | 24680.361 | 15471.024 | 586.52466 | 948.99081 |
| 2 | 35.71142 | 35.412321 | 27495.095 | 18590.685 | 744.52115 | 976.70178 |
| 3 | 33.436075 | 36.454169 | 26856.737 | 20644.978 | 859.3681 | 980.49189 |
| 4 | 31.567245 | 37.660292 | 26897.091 | 22370.263 | 996.695 | 990.61923 |
| 5 | 31.508465 | 37.738317 | 26947.85 | 22460.451 | 1005.9572 | 991.74025 |
| 6 | 30.780646 | 38.026215 | 26768.624 | 22670.973 | 1035.1694 | 992.0446 |
| 7 | 31.261411 | 38.026215 | 27080.448 | 22775.163 | 1040.16 | 995.65034 |
| 8 | 31.192997 | 38.139694 | 27141.391 | 22897.982 | 1053.9569 | 997.40882 |
| 9 | 30.832338 | 38.206982 | 26965.828 | 22894.456 | 1058.9004 | 996.05079 |
| 10 | 30.566525 | 38.302500 | 26909.063 | 22923.131 | 1067.7208 | 995.96924 |
| 11 | 30.622633 | 38.366159 | 26982.633 | 23014.313 | 1076.7212 | 997.66435 |
| 12 | 30.194766 | 38.576674 | 26957.814 | 23082.318 | 1097.3796 | 998.66932 |
| 13 | 30.091864 | 38.645529 | 26968.937 | 23109.213 | 1104.5003 | 999.27585 |
| 14 | 37.153348 | 33.487733 | 24680.361 | 15471.024 | 586.52466 | 948.99081 |

**TABLE 8.** Two optimal designs of the N boom with mass ≤ 1000 g.

| No. | $EI_x$ /(Nm$^2$/rad) | | $EI_x$ /(Nm$^2$/rad) | | $GJ_z$ /(Nm$^2$/rad | | *RE* /% | | |
|---|---|---|---|---|---|---|---|---|---|
| | RS results | FE results | RS results | FE results | RS results | FE results | $EI_x$ | $EI_y$ | $GJ_z$ |
| 3 | 26856.737 | 24960.113 | 20644.978 | 22018.728 | 859.3681 | 819.268 | 7.60 | -6.24 | -5.25 |
| 6 | 26768.624 | 28722.362 | 22670.973 | 21242.741 | 1035.1694 | 1118.058 | -6.80 | 6.72 | -7.41 |

## IV. MULTI-OBJECTIVE OPTIMIZATION DESIGN

The N boom should be designed for high stiffness deployment behavior to resist external disturbances. Bending stiffness around the $x$- and $y$-axis, and torsional stiffness around the $z$-axis are selected as the objectives. The mass of the N boom is directly related to the launch costs. Thus, mass is set as the constraint. The bonded web height $h$ and central angle $\theta_2$ of the middle tape spring are set as the design variables. Then, the multi-objective optimization design models of the N boom with three design objectives can be written as follows:

$$\begin{cases} \text{Opt.} \left\{ EI_x|_{\max} ; EI_y|_{\max} ; GJ_z|_{\max} ; \right\} \\ \text{S.t.} Mass \leq 1000g; \\ 30\text{mm} \leq h \leq 50\text{mm}; \\ 30^\circ \leq \theta_2 \leq 45^\circ. \end{cases} \tag{17}$$

According to the analysis in Section 3.2, it is found that bending stiffness around the $x$- and $y$- axes, torsional stiffness around the $z$-axis favor different design variables. Non-dominated sorting genetic algorithm II is applied to realize the optimal design with a population size of 50 and generation number of 48. The value of the objective function $T$ is equal to the sum of the objective components ($O_j$) with a corresponding weight factor ($W_j$) and scale factor ($S_j$) of the $j$-th objective component [26], i.e.,

$$T = \sum_{j=1}^{p} \frac{O_j \cdot W_j}{S_j} \tag{18}$$

where $j$ ($j = 1, 2, \ldots, q$) is the number of optimization objectives, and $q$ ($q = 4$) is the total number of objectives.

According to Eq.(18), the weight and scale factors of the objective component are equal, and the influences of the component with a small order of magnitude will be weaken. Given the significant bending stiffness around the $x$- and $y$-axes, both their scale factors are set to 1, and the weight factors are set to 0.5 and 0.8, respectively. Torsional stiffness $GJ_z$ of the N boom with an open cross section is weak, and $GJ_z$ is more important. Then, the scale and weight factors of the $GJ_z$ are set to 1 and 100, respectively. The order of magnitude of mass is small; hence, the weight factor is set to 20. The scale and weight factors of the objectives and constraint are selected and listed in Table 6.

The feasible designs of the N boom are depicted in Table 7. The two optimal designs, namely, Nos.3 and 6. Then, the FE models of the two optimal designs are constructed. The bending and torsional stiffness are listed in Table 8. Notably, the REs between the RS and FE results are no more than 7.6 %. Thus, the accuracies of the surrogate model are

verified again. However, No.6 is selected as the optimal design with $h = 30.780646$ mm and $\theta_2 = 38.026215°$ because the index of $GJ_z$ is dominated.

## V. CONCLUSIONS

The proposed N deployable boom concept consisted of three tape springs, wherein the middle tape spring had two circumscribed circles and two adjacent tape springs that bonded along one longitudinal edge of the C shapes. The post-buckling behaviors of the N boom under three different axial directions were analyzed using the nonlinear FE ABAQUS/Explicit solver.

The surrogate models for imperfection-sensitive quantities of interest of bending stiffness and torsional stiffness were derived from the quartic polynomials on the basis of RS method. A total of 25 sample points were created on the basis of the two-factor five-level full factorial DoE method. The precision of the surrogate models was validated by the absolute value of REs, which were no more than 8.81% in the entire design space.

The multi-objective optimization design was completed via the modified non-dominated sorting genetic algorithm II for the N boom. The optimal design configuration with the central angle $\theta_2 = 38.026215°$ and bonded web height $h = 30.780646$ mm possessed high torsional and bending stiffness values. The FE model of the selected optimal design was established, and the RE between its FE and RS results was no more than 7.6%.

The bending stiffness around the $x$-axis was sensitively to both the central angle $\theta_2$ and bonded web height $h$, but bending stiffness around the $y$-axis and torisonal stiffness around $z$-axis were more sensitive to the bonded web height $h$ than the central angle $\theta_2$ of the middle tape spring. A large bonded web height of the N boom should be selected to improve the torsional behavior and disturbance resistance capacity in the fully deployed state.

## REFERENCES


[1] C. Sickinger and L. Herbeck, "Deployment strategies, analyses and tests for the CFRP booms of a solar sail," in *Proc. Eur. Conf. Spacecraft Struct., Mater. Mech. Test.*, 2002, pp. 1–10.

[2] Y. Hu, W. Chen, J. Gao, J. Hu, G. Fang, and F. Peng, "A study of flattening process of deployable composite thin-walled lenticular tubes under compression and tension," *Compos. Struct.*, vol. 168, pp. 164–177, May 2017.

[3] J.-B. Bai, D. Chen, J.-J. Xiong, and R. A. Shenoi, "Folding analysis for thin-walled deployable composite boom," *Acta Astronautica*, vol. 159, pp. 622–636, Jun. 2019.

[4] J. Banik and T. Murphey, "Performance validation of the triangular rollable and collapsible mast," in *Proc. 24th Annu. AIAA/USU Conf. Small Satell.*, 2010, pp. 1–8.

[5] H. Yang, R. Liu, Y. Wang, Z. Deng, and H. Guo, "Experiment and multiobjective optimization design of tape-spring hinges," *Struct. Multidisciplinary Optim.*, vol. 51, pp. 1373–1384, Jun. 2015.

[6] A. Stabile and S. Laurenzi, "Coiling dynamic analysis of thin-walled composite deployable boom," *Compos. Struct.*, vol. 113, pp. 429–436, Jul. 2014.

[7] A. Hoskin, A. Viquerat, and G. S. Aglietti, "Tip force during blossoming of coiled deployable booms," *Int. J. Solids Struct.*, vols. 118–119, pp. 58–69, Jul. 2017.

[8] R. Zhang, X. Guo, Y. Liu, and J. Leng, "Theoretical analysis and experiments of a space deployable truss structure," *Compos. Struct.*, vol. 112, pp. 226–230, Jun. 2014.

[9] Z.-Y. Chu, J. Hu, S. B. Yan, and M. Zhou, "Experiment on the retraction/deployment of an active–passive composited driving deployable boom for space probes," *Mech. Mach. Theory*, vol. 92, pp. 436–446, Oct. 2015.

[10] Z. Chu and Y. Lei, "Design theory and dynamic analysis of a deployable boom," *Mech. Mach. Theory*, vol. 71, pp. 126–141, Jan. 2014.

[11] F. Li, J. Liu, G. Wen, and J. Rong, "Extending SORA method for reliability-based design optimization using probability and convex set mixed models," *Struct. Multidisciplinary Optim.*, vol. 59, no. 4, pp. 1163–1179, 2019.

[12] Z. Wang, J. Bai, A. Sobey, J. Xiong, and A. Shenoi, "Optimal design of triaxial weave fabric composites under tension," *Compos. Struct.*, vol. 201, pp. 616–624, Oct. 2018.

[13] H. Chen, L. Li, W. Zhang, R. Liu, and S. Jiang, "A vibratory conveying method for planetary regolith: Preliminary experiment and numerical simulation," *IEEE Access*, vol. 7, pp. 29386–29396, 2019.

[14] G. Li, H. Huang, H. Guo, and B. Li, "Dynamic modeling and control for a deployable grasping manipulator," *IEEE Access*, vol. 7, pp. 23000–23011, 2019.

[15] H. M. Y. C. Mallikarachchi and S. Pellegrino, "Design of ultrathin composite self-deployable booms," *J. Spacecraft Rockets*, vol. 51, no. 6, pp. 1811–1821, 2014.

[16] F. Liu, D. Jin, and H. Wen, "Optimal vibration control of curved beams using distributed parameter models," *J. Sound Vib.*, vol. 384, pp. 15–27, Dec. 2016.

[17] H. M. Y. C. Mallikarachchi, "Predicting mechanical properties of thin woven carbon fiber reinforced laminates," *Thin Walled Struct.*, vol. 35, pp. 297–305, Feb. 2019.

[18] J. E. Sader, M. Delapierre, and S. Pellegrino, "Shear-induced buckling of a thin elastic disk undergoing spin-up," *Int. J. Solids Struct.*, vol. 166, pp. 75–82, Jul. 2019.

[19] C. Leclerc, A. Pedivellano, and S. Pellegrino, "Stress concentration and material failure during coiling of ultra-thin TRAC booms," in *Proc. AIAA*. Orlando, FL, USA: SciTech, 2018, p. 0690.

[20] C. Leclerc, L. L. Wilson, M. A. Bessa, and S. Pellegrino, "Characterization of ultra-thin composite triangular rollable and collapsible booms," in *Proc. AIAA*. Grapevine, TX, USA: SciTech, 2017.

[21] M. A. Bessa and S. Pellegrino, "Design of ultra-thin shell structures in the stochastic post-buckling range using Bayesian machine learning and optimization," *Int. J. Solids Struct.*, vols. 139–140, pp. 174–188, May 2018.

[22] M. A. Bessa, R. Bostanabad, Z. Liu, A. Hu, D. W. Apley, C. Brinson, W. Chen, and W. K. Liu, "A framework for data-driven analysis of materials under uncertainty: Countering the curse of dimensionality," *Comput. Method. Appl. Mech. Eng.*, vol. 320, pp. 633–667, Jun. 2017.

[23] F. Roybal, J. Banik, and T. Murphey, "Development of an elastically deployable boom for tensioned planar structures," in *Proc. 48th AIAA/ASME/ASCE/AHS/ASC Struct., Struct. Dyn., Mater. Conf.*, 2012, p. 1838.

[24] H. Ye, Y. Zhang, Q. Yang, Y. Xiao, R. V. Grandhi, and C. C. Fischer, "Optimal design of a three tape-spring hinge deployable space structure using an experimentally validated physics-based model," *Struct. Multidisciplinary Optim.*, vol. 56, pp. 973–989, Sep. 2017.

[25] H. Yang, H.-W. Guo, Y. Wang, R. Q. Liu, and M. Li, "Design and experiment of triangular prism mast with tape-spring hyperelastic hinges," *Chin. J. Mech. Eng.*, vol. 31, May 2018, Art. no. 33.

[26] H. Yang, L. Liu, H. Guo, F. Lu, and Y. Liu, "Wrapping dynamic analysis and optimization of deployable composite triangular rollable and collapsible booms," *Struct. Multidisciplinary Optim.*, vol. 59, pp. 1371–1383, Apr. 2019.